Journal of Thermal Science Vol.24, No.5 (2015) 410−416

DOI: 10.1007/s11630-015-0803-1 **Article ID: 1003-2169(2015)05-0410-07**

Performance and Internal Flow of a Counter-rotating Type Tidal Stream Turbine

Bin Huang and Toshiaki Kanemoto

Faculty of Engineering, Kyushu Institute of Technology, Sensui 1-1, Tobata, Kitakyushu 804-8550, Japan

In the past decade, the tidal energies have caused worldwide concern as it can provide regular and predictable renewable energy resource for power generation. The majority of technologies for exploiting the tidal stream energy are based on the concept of the horizontal axis propellers, which can be derived from the design and operation of wind turbines. However, there are some peculiar features such as the propeller working in the seawater with free surface and the possible occurrence of cavitation as compared with wind turbines. Especially, for a counter-rotating type tidal stream power turbine, it is difficult to accurately predict the interaction between the front and rear blades at the design stage by blade element momentum theory. As a result, CFD shows its advantage to predict the performance of counter-rotating type propellers of the tidal stream turbine. In order to improve the accuracy of CFD predictions, the predicted results must be verified with experimental values. In this paper, a CFD model using block-structured grid was set up and experimental test was performed in a water tunnel for a tidal stream turbine with counter-rotating type propellers. The comparison between CFD predictions and experimental data shows quite good agreement on the power coefficients, which provides an evidence of validation of the CFD model. Such results offer the necessary confidence in the accuracy of the set up CFD model for the counter-rotating type tidal stream turbine.

Keywords: Counter-rotating, tidal stream turbine, internal flow, CFD, experimental validation

Introduction

Climate change and global warming concerns, coupled with high oil prices, peak oil, and increasing government support, are driving increasing renewable energy legislation, incentive and commercialization [1]. The occurrence of PM2.5 pollution has been raising public concern for coal's environmental and health impacts, which plays a large role in restricting coal demand [2]. The energy regulators all over the world have increasingly realized the importance of tapping into the renewable energy market.

Renewable energy is generally defined as energy that comes from resources which are naturally replenished on a human timescale such as biomass energy, geothermal energy, hydropower energy, marine energy, solar energy and wind energy [3]. As for the fluid energy resources in the world, the hydropower resource of about 2 TW can be exploited newly at the onshore, the wind resource of about 72 TW and the ocean resource more than $2x10^3$ TW can be also exploited [4]. That is, the ocean resource as a kind of endless energy resource shows great potential to be harnessed in different ways. The forms of ocean energy can be categorized into tidal, wave, current, thermal gradient and salinity gradient, which requires respectively different technologies for energy conversion [5].

Received: March 2015
Bin Huang: Project Assistant Professor

Nomenclature

A	propeller area (m^2)	λ	tip speed ratio
C_p	power coefficient	ρ	fluid density (kg/m^3)
d	propeller diameter (m)	ω	rotating speed (rad/s)
R	blade tip radius (m)	β	blade pitch angle (°)
T	torque ($N{\cdot}m$)	**Subscripts**	
V_{in}	inlet speed (m/s)	F	front propeller
Z	Number of blades	R	rear propeller
Greek letters		T	tandem propellers

One such major form of this sustainable energy is the tidal stream energy, which converts the kinetic energy to electric power. Tidal stream generators draw energy from water in much the same way as wind turbines draw energy from air. However, the potential for power generation by an individual tidal turbine can be greater than that of similarly rated wind energy turbine. The higher density of water relative to air (water is about 800 times the density of air) means that a single generator can provide significant power at slow tidal flow velocity as compared with similar wind velocity [6]. As a result, the horizontal-axis tidal stream turbine (HATST) has been proposed as a cost-effective turbine to harness energy from tidal stream [7].

Much of the design technologies associated with HATSTs can be derived from the wind industry due to their similar working principles [8]. Nevertheless, there are some different characteristics such as the effects of the free surface, the different levels of Reynolds number and turbulence, the different stall characteristics as well as the possible occurrence of cavitation which should be taken into consideration in the design process of a tidal turbine [9]. However, the blade element momentum (BEM) theory has been proven to be well established for modeling rotor dynamics of not only wind but also marine propellers [10]. Recently, Batten and Bahaj et al. [11-14] have employed the developed BEM theory to the hydrodynamic design of marine current turbines, which shows good agreement between the numerical results and experimental data obtained from tests of an 800mm diameter model turbine carried out in a cavitation tunnel and a towing tank.

The counter-rotating type HATSTs with both mooring and pile systems have been proposed in previous works [15, 16] as shown in Fig. 1. However, for a counter-rotating type HATST, it is difficult to accurately predict the interaction between the front and the rear blades by blade element momentum theory. As a result, CFD shows its advantage to predict the performance of a counter-rotating type HATST. This paper describes the CFD analysis and the experimental measurements of a model counter-rotating type HATST. Detailed comparisons between the CFD predictions and experimental results are presented to provide an evidence of validation of the CFD model.

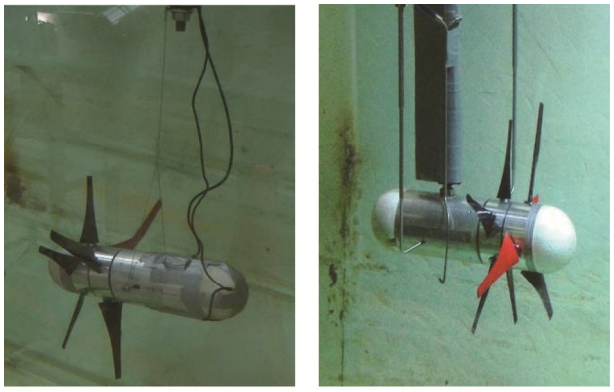

(a) Mooring type (b) Pile type

Fig. 1 Model counter-rotating type HATSTs

Description of model turbine

A model counter-rotating type HATST with the diameter of 500 mm was designed as a trade-off between maximizing the Reynolds number and not incurring excessive tunnel blockage correction [12, 13]. The blade profiles were composed of the blade element KIT001 with three different relative thicknesses as shown in Fig. 2. The chord, the pitch angle and the thickness distributions of the model counter-rotating type blades are shown in Fig. 3. Profiles matching the same thickness as described in Fig. 3 were then obtained by interpolating from the three original blade elements as shown in Fig. 2.

The diameter of the front propeller is 500mm and the rear propeller is 450 mm, namely the diameter ratio [$=d_R/d_F$] is 0.9. The number of blades for the front and the rear propellers are Z_F = 3 and Z_R = 5, respectively. The axial distance between both propellers is set to 80mm, and the diameter of the hub is set to 90 mm.

CFD model

The CFD model was set up using ANSYS CFX14.0 which solves three-dimensional Reynolds-averaged Navier-Stokes equations. The computational domain consisted of

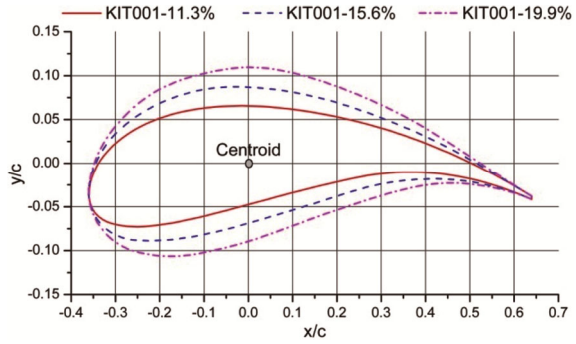

Fig. 2 Blade element KIT001 with three different relative thicknesses

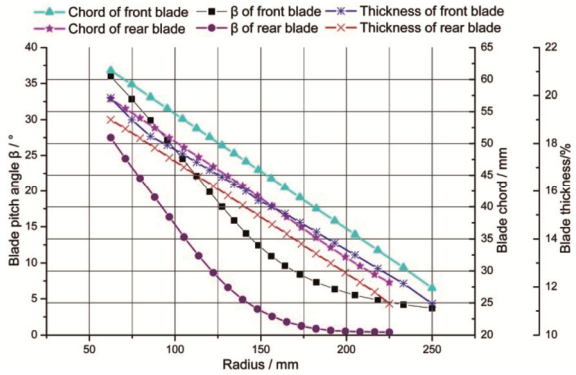

Fig. 3 Blade profile specifications of the counter-rotating type blades

three parts: the front rotor, the rear rotor and the stator. The length of the stator domain was set to $10d_F$, in which $3d_F$ and $7d_F$ for the upstream and the downstream of the front propeller respectively. To keep similar to the experimental conditions in the water tunnel, the width and depth were 1500mm and 1200mm, respectively. The model unit was placed closing to the water surface when the tip of front blade was 100mm submerged. The diameters of the front and rear rotor domains were both modeled with $1.1d_F$. The flow was simulated around the model unit mounted with not only the pile but also the mooring cable.

A block structured hexahedral grid method in ICEM CFD was employed to generate mesh for all the computational domains. A C-mesh was applied to each layer of the blades since it fits well for the hydrofoil shape of the blades. The front rotor block and the rear rotor block were built in a 120° segment and 72° segment which both include only one blade as shown in Fig. 4. The refined grids were concentrated in regions of importance such as around the blades and towards and away from the tip to give $y+ < 50$ on the blade surfaces. Table 1 presents the mesh statistics of every computational domain.

The mesh created above was then imported into CFX and copied around the rotational axis to simulate the full turbine. The k-ω SST model in ANSYS CFX was used in the current study to solve the incompressible Reynolds-average Navier-Stokes equations. The stream normal velocity (V_{in}=1m/s) and the averaged static pressure (P= 0Pa) were prescribed as the boundary conditions at the inlet and outlet of computational domains, respectively. A symmetry boundary condition was given on the top to simplify the free surface in experimental condition. The smooth and no-slip walls were imposed on the other solid surfaces. To simplify the simulations and reduce computational cost, only single front blade and the single rear blade were placed in the domain assuming rotational periodic interface between the adjacent blades. The stage method which performs a circumferential averaging of the fluxes through the bands on the interface was used for the connection between each computational domain. The convergence criterion was set as the maximum values of the residuals reaching 10^{-4}.

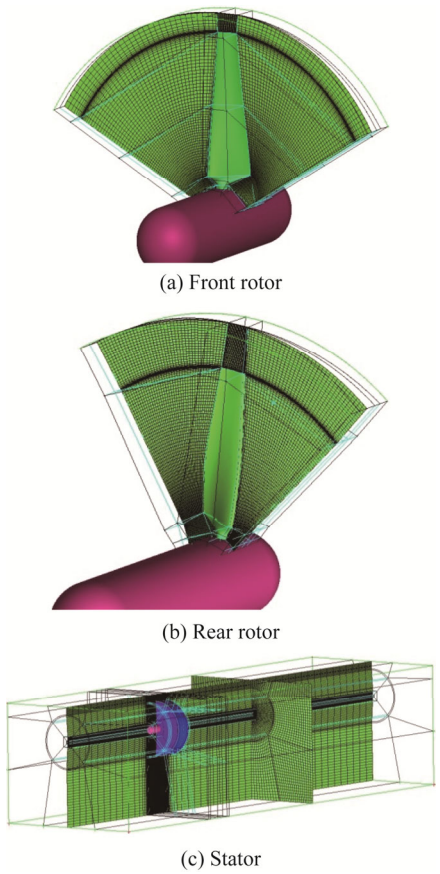

Fig. 4 Blocking strategy and mesh distributions of the computational domains

Table 1 Mesh statistics for every computational domain

Domain	Front rotor	Rear rotor	Stator
Number of elements	605870	695676	681720
Number of nodes	632418	723720	700832
Number of blocks	91	74	175

In the counter-rotating type propellers, the radius of the front propeller was selected as reference variable, so

the tip speed ratios (TSRs) and power coefficients were defined as follows:

$$\lambda_F = \frac{\omega_F R_F}{V_{in}} \tag{1}$$

$$\lambda_R = \frac{\omega_R R_F}{V_{in}} \tag{2}$$

$$\lambda_T = \lambda_F + \lambda_R \tag{3}$$

$$C_{PF} = \frac{T_F \omega_F}{(1/2)\rho V_{\text{in}}^3 A_F} \tag{4}$$

$$C_{PR} = \frac{T_R \omega_R}{(1/2)\rho V_{\text{in}}^3 A_F} \tag{5}$$

$$C_{PT} = C_{PF} + C_{PR} \tag{6}$$

Experimental methodology

Experiments for the model counter-rotating type HATST were carried out in a circulating water tunnel at West Japan Fluid Engineering Laboratory Co., Ltd. The tunnel has a working section of 1.2m×1.5m (depth×width) and an opening top surface. The model turbine was fixed and the water was driven by two external propellers to simulate the real marine environment. The stream velocity was measured at locations upstream of the front blade using two pitot tubes. In this experiment, the flow velocity was fixed at 1m/s. The experimental apparatus in the water tunnel is shown in Fig. 5. The tandem propellers were connected to an isolated motor with an inverter system, respectively, in place of the peculiar generator with double rotational armatures. Both rotational speeds were adjusted to make the rotational torque of the front propeller coincide with the torque of the rear propeller [17].

Comparison between CFD and experiment

The performance in terms of the power coefficient C_{PT} of the model counter-rotating type HATST predicted by the CFD model is compared with experimental data, as shown in Fig. 6, where λ_T is the relative tip speed ratio (TRS). It can be seen that the trend of the power coefficient shows good agreement for the entire TSR region, and the best efficiency point (BEP) occurs during the region λ_T = 5~6 for both CFD and experimental results. However, the CFD model seems a general tendency to over predict the power coefficient throughout the entire TSR region. This tends to be more evident in the high TSR region. It may be caused by the effects of the waving free surface close to the propeller and the complex interaction (the interface in the simulation) between both propellers. Fig. 7 illustrates the respective power coeffi-

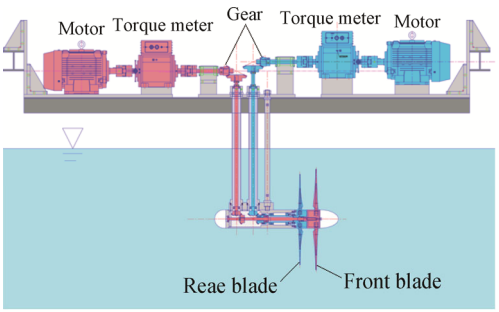

(a) Schematic diagram

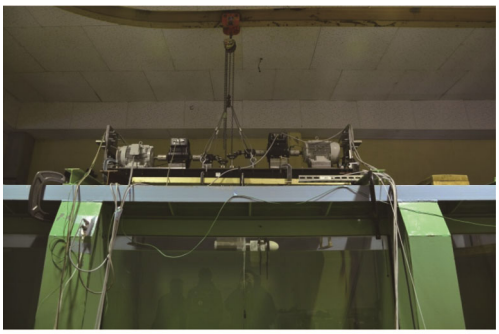

(b) Photograph

Fig. 5 Layout of experimental apparatus in the water tunnel

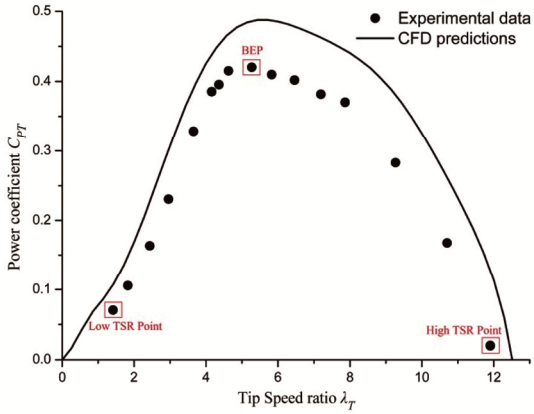

Fig. 6 Comparison of power coefficient between CFD and experiment

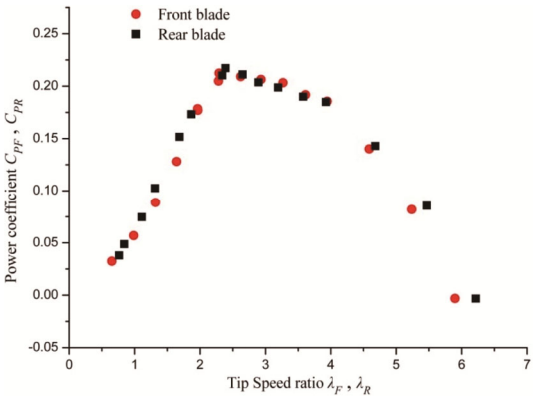

Fig. 7 Comparison of power coefficient between front propeller and rear propeller

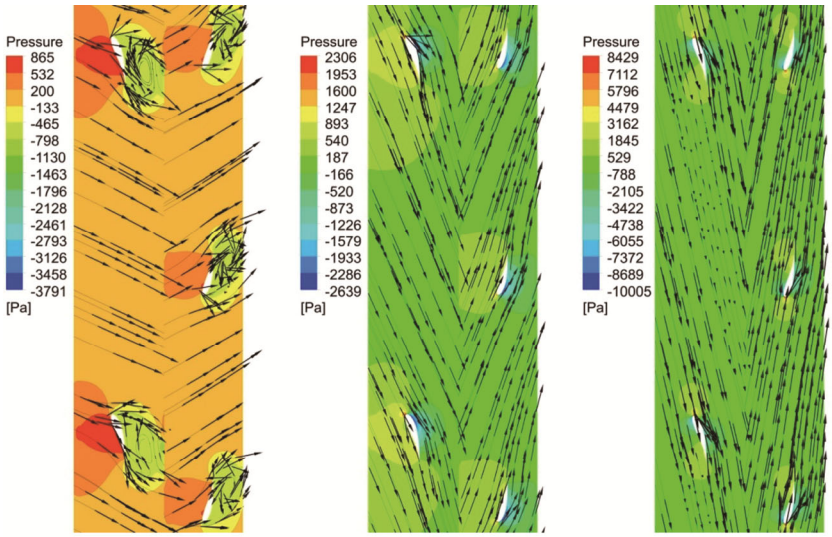

(a) Low TSR Point (b) BEP (c) High TSR Point

Fig. 8 Streamline and pressure distributions on S1 surface at 50% spanwise position

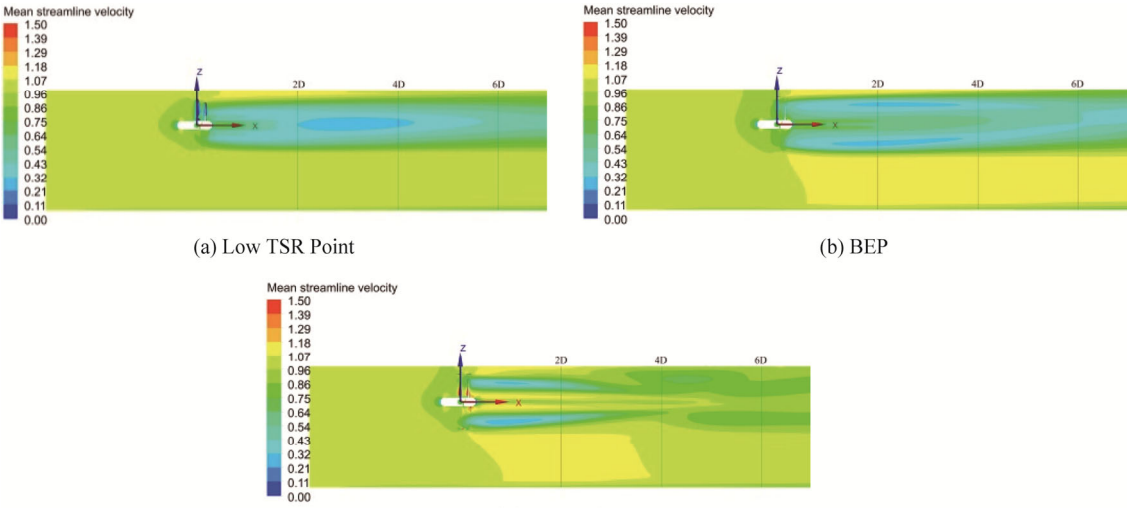

(a) Low TSR Point (b) BEP

(c) High TSR Point

Fig. 9 Contours of mean streamwise velocity on plane through center of domain

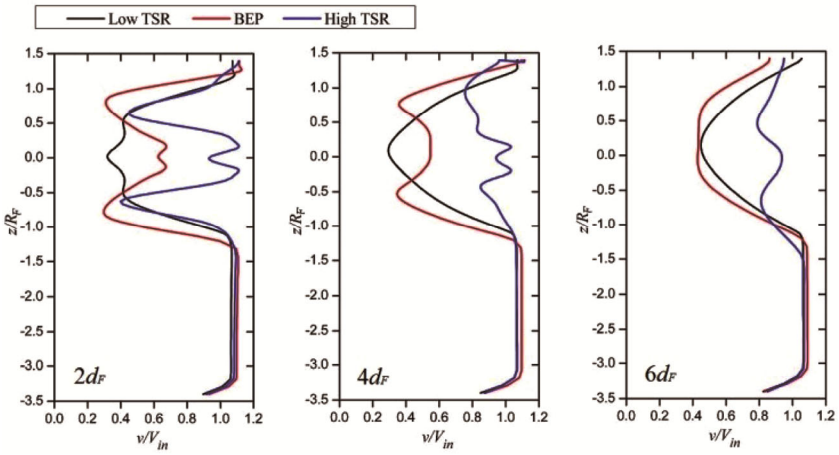

Fig. 10 Normalized mean streamwise velocity profiles at distances downstream of the turbine

cient of the front and the rear propellers. The similar performance between both propellers gives an additional confidence in the developed counter-rotating type HATST.

Internal flow analysis

Figure 8 shows the relative streamline and pressure distributions on S1 surface at 50% spanwise position for three different conditions marked in Fig. 6. At low TSR point, the flow exhibits significant separation and detached vortex on the suction surface of the blade. At this condition, the serious stall phenomenon leads to decrease in the power coefficient. At BEP condition, the streamlines keep smooth and fully attached to the blade surfaces, and then the suitable angle of attack guarantees good performance. At high TSR point, the stagnation point moves to the suction side resulting in low lift.

Fig. 9 shows the contours of mean streamwise velocity on the vertical plane through the center of the propeller shaft. It can be seen that the largest velocity defect moves from the center to the tips of the blades as the TSR increases. It is also observed that the higher TSR leads to a faster recovery of the streamwise velocity. In order to investigate the wake characteristics more intuitively, the mean streamwise velocity profiles normalized with the inlet velocity are shown in Fig. 10 at distances $2d_F$, $4d_F$ and $6d_F$ downstream measured from the section of the front propeller. It is clear that the mean streamwise velocity recovers fastest at high TSR point, exceeding 80% recovery rate after $4d_F$ downstream. However, it shows intensive instability at high TSR point. And the mean streamwise velocity recovers slowly at both low TSR and BEP conditions, with only 40% ~ 60% recovery rates at $6d_F$ downstream. Noticeably, for the purpose of improving the calculation accuracy, the downstream domain should be extended to weaken the blockage effect of the outlet.

Conclusions

This paper presents the CFD simulations and experimental analysis of a counter-rotating type tidal stream turbine. Over a range of TSRs, the trend of the power coefficient predicted by the CFD model has been found to compare well with the experimental data, although the CFD model has a general tendency to over predict the power coefficient.

The internal flow and wake characteristics are also presented. At the best efficiency point, the smooth streamlines and the suitable angle of attack around the blade demonstrate good confidence in the design of the model turbine. The separated flow and the inappropriate stagnation point at off design conditions lead to decrease in the power coefficient. In the wake, the mean streamwise velocity defect recovers fastest with intensive instability at high TSR point. However, only 40% ~ 60% recovery rates have been obtained at $6d_F$ downstream measured from the section of the front propeller.

Acknowledgement

The authors wish to thank to Dr. Yuta Usui and Mr. Kohei Takaki who graduated from Kyushu Institute of Technology, Japan. Some parts of the researches were co-sponsored by the New Energy and Industrial Technology Development Organization in Japan, and Research Project: Grant-in-aid for Science Research C in Japan (2012-2014).

References

[1] Greenwood, C., Hohler, A., Hunt, G.: Global Trends in Sustainable Energy Investment 2007: Analysis of Trends and Issues in the Financing of Renewable Energy and Energy Efficiency in OECD and Developing Countries. http://www.unep.org/. United Nations Environment Programme, (2007).

[2] Fang, L.F.: The Myth of China's Endless Coal Demand. http://www.greenpeace.org/usa/en/media-center/reports/Myth-of-China-Endless-Coal-Demand/. Greenpeace USA, (2013).

[3] Ellabban, O., Abu-Rub, H., Blaabjerg, F.: Renewable energy resources: Current status, future prospects and their enabling technology, Renewable and Sustainable Energy Reviews, Vol. 39, pp.748–764, (2014).

[4] World Energy Council, 2010 Survey of Energy Resources. http://www.worldenergy.org/wp-content/uploads/2012/09/ser_2010_report_1.pdf. (Nov., 2010,)

[5] Bedard, R., Jacobson, P.T., Previsic, M., Musial, W., and Varley, R.: An overview of ocean renewable energy technologies, Oceanography, Vol. 23, No. 2, pp.22–31, (2010).

[6] http://en.wikipedia.org/wiki/Tidal_stream_generator.

[7] Fraenkel, P.: Power from marine currents, Proc IMechE Part A: J. Power and Energy, Vol. 216, No. 1, pp.1–14, (2012).

[8] Ben Elghali, S.E., Benbouzid, M., Charpentier, J.F.: Marine tidal current electric power generation technology: state of the art and current status, IEEE International electric machines & drives conference, Antalya, Turkey, pp. 1407–1412, (2007).

[9] Batten, W.M.J., Bahaj, A.S., Molland, A.F., Chaplin, J.R.: Hydrodynamics of marine current turbines, Renewable Energy, Vol. 31, No. 2, pp.249–256, (2006).

[10] Burton, T., Sharpe, D., Jenkins, N., Bossanyi, E.: Wind energy handbook, Chichester: Wiley, (2000).

[11] Batten, W.M.J., Bahaj, A.S., Molland, A.F., Chaplin, J.R.: Experimentally validated numerical method for the hydrodynamic design of horizontal axis tidal turbines, Ocean Engineering, Vol. 34, No.7, pp.1013–1020, (2007).

[12] Bahaj, A.S., Molland, A.F., Chaplin, J.R., Batten, W.M.J.: Power and thrust measurements of marine current turbines under various hydrodynamic flow conditions in a cavitation tunnel and a towing tank, Renewable Energy, Vol. 32, No. 3, pp.407–426, (2007).

[13] Bahaj, A.S., Batten, W.M.J., McCannb, G.: Experimental verifications of numerical predictions for the hydrodynamic performance of horizontal axis marine current turbines, Renewable Energy, Vol. 32, No. 15, pp.2479–2490, (2007).

[14] Batten, W.M.J., Bahaj, A.S., Molland, A.F., Chaplin, J.R.: The prediction of the hydrodynamic performance of marine current turbines, Renewable Energy, Vol. 33, No. 5, pp.1085−1096, (2008).

[15] Usui, Y., Kanemoto, T., Hiraki, K.: Counter-Rotating Type Tidal Stream Power Unit Boarded on Pillar (Performances and Flow Conditions of Tandem Propellers), Journal of Thermal Science, Vol. 22 No. 6, pp.580−585, (2013).

[16] Usui, Y., Takaki, K., Kanemoto, T., Hiraki, K.: Counter-rotating type tidal-stream power unit playing favorable features in various ocean circumstances, IMECE2013, San Diego, California, USA, (2013).

[17] Suzuki, T and Kanemoto, T.: Counter-Rotating Type Tidal Range Power Unit, Journal of Energy and Power Engineering, Vol.7, No. 12 (2013, Dec), pp.2381–2387.